

Petrography and mineralogy of calcium-, aluminum-rich inclusions in an unequilibrated carbonaceous chondrite Y 81020 (CO3.05)

Ritesh Kumar Mishra^{1,2,*}

¹Center for Isotope Cosmochemistry and Geochronology, Astromaterials Research and Exploration Science Division, EISD-XI, NASA-Johnson Space Center, 2101, NASA Parkway, Houston, TX 77058, USA

²Oak Ridge National Laboratory Associated Universities, Tennessee 37830, Kentucky, USA

Petrographic and quantitative analyses of more than 70 refractory inclusions found in the studied thin section of Yamato 81020 (CO3.05) showed diverse objects that can be grouped into five distinct types based on morphology and mineralogy. Mineralogical, textural similarities to the pristine carbonaceous vigarano (3.1–3.4) types of Efremovka, Vigarano were observed despite their smaller size (~100 micron diameter). Wark-Lovering rims were found predominantly in melilite-rich calcium, aluminum-rich inclusions. Comparison of mineralogy, morphology at macro and micro scale of Y 81020 with ALH A77307 and other carbonaceous chondrites is suggestive of the unaltered characteristics of the refractory inclusions in agreement with previous studies.

Keywords: Antarctic meteorites, calcium, aluminum-rich inclusions, petrography, quantitative analyses, unequilibrated carbonaceous chondrites.

ASTEROIDS and comets are repositories of the early solar system solids that escaped aggregation into larger planetesimals and planetary bodies. Some of these objects, on perturbation, lose their gravitationally stable path around the Sun and crash on the Earth as ‘meteorites’. Several asteroids that were small enough did not possess enough internal heat to undergo any differentiation and hence have been able to preserve the earliest solar system solids in almost their original forms. Calcium, aluminum-rich inclusions (CAIs) found in these undifferentiated ‘chondritic’ meteorites represent the earliest formed solar system solids that have been absolutely dated using Pb–Pb absolute chronometer to ~4568 Ma (refs 1, 2). CAIs are found in all types of chondrites but their abundance, typical/mean size, morphological and mineralogical characteristics differ quite significantly between different clans/groups^{3–6}. The quintessential large (few mm – few cm) type B’s are found almost exclusively in the carbonaceous vigarano (CV) type of Efremovka (~3.1–3.4), Vigarano (~3.1–3.4), Allende (>3.6),

etc. From initial studies until recent times, most studies have been carried out in these substantial larger objects of CV chondrites primarily hindered by analytical techniques and facilitated by their relatively simple igneous character^{6–13}. Certainly, quite a lot has been learnt from studies of these objects, but on the other hand they are neither the true representatives nor the best preserved samples^{6–10}. It is important to note that only in recent times, techniques have been developed to identify the pristine characters and utilize them to identify only a few of the least altered meteorites^{14–17} available in our collections around the world. In this paper, I describe the petrology and mineralogical characterization of CAIs and other refractory inclusions in an Antarctic ‘find’ of Yamato 81020 that belongs to Carbonaceous ‘Ornans’ (CO). The study identifies differences in morphology, abundance, modal abundance of mineral phases in CAIs of similar kinds (CO) and other groups of meteorites studied previously. The oxygen isotopic compositions and short-lived chronology (²⁶Al–²⁶Mg) studies of some of the larger objects of interest will be presented in a following paper.

Sample and analytical technique

Yamato (Y) 81020 is an Antarctic ‘find’ of ~270 g that was collected by Japanese expedition in 1981 near ‘Yamato hills’ in the northern regions of Antarctica. It is classified as carbonaceous chondrite of ‘Ornans’ type and has been re-classified to one of the lowest petrologic types of 3.05 (ref. 14). Petrographic classification of 3.05 inferred from textures, compositions of mineral phases in matrices, vitreous nature of glassy mesostases in chondrules, micro-Raman studies of insoluble organic matter imply that most components of this meteorite have not experienced temperatures exceeding 300°C in the nebula and parent body after their formation and aggregation into the parent body^{14–17}. It therefore belongs to an important and very rare category of meteorites like Semarkona (LL3.00), QUE 99177 (CR3.0), ALH A77307 (CO3.03), and has best preserved (least altered) pristine samples of

*e-mail: riteshkumarmishra@gmail.com

the early solar system solids. A thin section (#41-3) of $\sim 32 \text{ mm}^2$ taken on loan from Antarctic meteorite collection of National Institute of Polar Research (NIPR), Tokyo was examined in the present study. X-ray elemental abundance maps of major (calcium, magnesium, aluminium, iron, sulphur) and minor elements (nickel, sodium, chromium, etc.) of the meteorite thin section were obtained using JEOL 8530 F field emission electron microprobe at NASA-Johnson Space Centre, Houston. A focused electron beam of $\sim 70 \text{ nA}$ and beam size of $\sim 1 \mu\text{m}$ were rastered over the sample and the X-ray spectrum was collected in energy dispersive mode. Mosaic (false) colour composite maps of different elements were made that helped identify bulk characteristics of different objects. High resolution maps of several objects of interest were subsequently obtained for a detailed study. In the thin section more than ~ 70 refractory inclusions, CAIs and amoeboid olivine aggregates (AOAs) and several Al-rich chondrules were found. Several other smaller, fragmented Ca-, Al-rich objects of $< 2 \mu\text{m}$ size were also found in the thin sections. However, only refractory inclusions larger than $\sim 65 \mu\text{m}$ were considered for discussion and comparative studies. The smaller objects are mostly fragmented remains of larger objects and do not affect the conclusions of the study. Quantitative analyses of phases of interest were carried out using a $\sim 15 \text{ nA}$ focused e-beam of 15 kV in wavelength dispersive mode. Spectrometers were calibrated and analogous terrestrial standards were measured for accurate determination of phases of interests in the objects present in the thin section of the meteorite. Five spectrometers having crystals of LiF, PET, LLiF, LPET and TAP were used such that Na and K were measured first for 15 sec, while background counts were measured for 10 sec. For other elements measurement time was 30 sec and background counts were measured for $\sim 20\text{--}30$ sec. ZAF procedure was used for matrix correction.

Results

About 70 refractory inclusions mostly consisting of Ca-, Al-rich refractory inclusions were found in Y 81020 along with several smaller fragmented objects of similar mineralogical composition. The larger ones with sizes $> 65 \mu\text{m}$ are shown in Table 1 with their size, typical mineralogy and other features. Figures 1–3 show back-scattered electron images of these objects and magnified images of regions of interests.

General features

The typical abundance of refractory inclusions is similar to those reported in previous studies of CO^{11–13} and quite similar to CM (Mighei kind), CR (Renazzo) and other types of carbonaceous chondrites^{5,7}. Most refractory in-

clusions are typically smaller in size with an average size of $\sim 150 \mu\text{m}$ (Table 1, Figures 1–3). The typical sizes of refractory inclusions are similar to those present in CM and CR, but are smaller than those present in CV chondrites. However, few larger ones up to $\sim 450 \mu\text{m}$ are present. Generally speaking most are fragmented and also fractured (Figures 1–3). Most also have several perforations within them. Typically, the perforations are present above the spinel layer in the rim while also being present in other regions (Figure 3). As reported earlier, there is very limited aqueous alteration and cross cutting veins are seldom present^{13–15}. The refractory inclusions show diverse mineralogy that can be broadly grouped into five types based on their morphology and modal mineral composition which are described in detail in the following sections. These diverse groups show mineral compositions consisting of spinel, melilite, perovskite, pyroxene, anorthite, Fe, Ni metal, olivine and rare hibonite.

Classification criterion and types

The refractory inclusions can be classified into five different types based on the abundance of primary mineral assemblages and morphology: (1) Melilite-rich type, (2) Spinel, melilite, pyroxene bearing, (3) Spinel, pyroxene bearing, (4) Spinel, pyroxene, anorthite bearing, (5) Hibonite, pyroxene bearing.

The abundances of these different types of CAIs in the studied thin section follow the trend of the order of listing (Table 1). Only two hibonite inclusions of ~ 100 micron size were found. Uncharacteristically though, their peripheries have been altered to an unidentified, Ca, Fe, Mg, Zn, S rich phase. Y 81020 has been studied previously for mineralogical, isotopic studies of its different components^{13–18}. These petrographic observations are in agreement with previous studies of this meteorite^{13,18}. Figures 1–3 show the back-scattered electron images of a few objects representing the range of objects found in Y 81020.

Melilite-rich type CAIs

Several large CAIs present in the thin section are of this type (#1, 18, 20) and are shown in Figures 1–3. These CAIs have compact igneous texture. Their bulk compositions are akin to type ‘A’ dominated by preponderance of Al-rich melilite lying closer to the gehlenite end⁵. In the conventional classification scheme, these would be classified as compact type ‘A’s. Most of these CAIs have rims quite similar to Wark-Lovering rims, discussed in detail in the following sections. On spinel projected CMAS diagram⁵ the composition of lateral and transverse transects across larger CAIs (e.g. 18, 20, 1) lie closer to the Al₂O₃ apex above the normal bulk condensation trend line of type ‘A’, suggesting that melilite in these are of

Table 1. Properties and characteristic features of CAIs, AOAs and Al-rich chondrules in Y 81020 (CO3.05)

| Inclusion # | Shape | Size (μm) | Type | Accretionary rim | WL rim | Major phases | Minor phases | Perovskite abundance |
|---------------------|-------------|------------------------|--------------------|------------------|--------|------------------|--|----------------------|
| CAI 1 | Rectangular | 175 × 100 | Melilite-rich | No | Yes | Melilite | Spinel | Few |
| CAI 2 | Irregular | 100 × 50 | Sp–Mel–Px | No | No | Spinel, melilite | Pyroxene | Abundant |
| CAI 3 | Irregular | 100 × 70 | Sp–Mel–Px | No | No | Spinel, melilite | Pyroxene | Abundant |
| CAI 4 | Irregular | 120 × 120 | Sp–Mel–Px | No | Yes | Spinel, melilite | Pyroxene | Rare |
| CAI 5 | Ellipsoid | 180 × 120 | Sp–An–Px | Yes | Yes | Spinel | Anorthite, pyroxene | Absent |
| 6 Al-rich chondrule | Square | 290 × 120 | Ol–Plag | No | No | Olivine | Plagioclase | Absent |
| 7 AOA | Irregular | 290 × 130 | AOA | No | No | Olivine | Plagioclase | Absent |
| CAI 8 | Irregular | 120 × 124 | Melilite-rich | Yes | Yes | Melilite | Spinel | Rare |
| CAI 9 | Irregular | 200 × 130 | Sp–Mel–Px | No | No | Spinel, melilite | Pyroxene | Absent |
| CAI 10 | Irregular | 160 × 130 | Sp–An–Px | No | No | Spinel | Anorthite, pyroxene | Absent |
| CAI 11 | Rectangular | 160 × 130 | Melilite-rich | No | Yes | Melilite | Spinel | Abundant |
| CAI 12 | Shoe | 130 × 120 | Melilite-rich | Yes | Yes | Melilite | Spinel | Abundant |
| Inclusion 13 | Square | 65 × 60 | AOA | No | No | Olivine | Pyroxene | Absent |
| CAI 14 | Rod | 120 × 30 | Sp–Px | No | No | Spinel | Pyroxene | Abundant |
| CAI 15 | Irregular | 65 × 30 | Sp–Mel–Px | Yes | Yes | Spinel, melilite | Pyroxene | Rare |
| CAI 16 | Drop | 145 × 75 | Sp–An–Px | Yes | Yes | Spinel | Anorthite, pyroxene | Absent |
| CAI 17 | Bone | 130 × 120 | Sp–Mel–Px | Yes | Yes | Spinel, melilite | Pyroxene | Rare |
| CAI 18 | Circle | 235 × 195 | Melilite-rich | No | Yes | Melilite | Spinel | Abundant |
| CAI 19 | Rectangular | 200 × 110 | Sp–An–Px | No | No | Spinel | Anorthite, pyroxene | Absent |
| CAI 20 | Semi circle | 450 × 245 | Melilite-rich | Yes | Yes | Melilite | Spinel | Abundant |
| CAI 21 | Vase/cup | 85 × 75 | Sp–Mel–Px | Yes | Yes | Spinel | Pyroxene | Rare |
| Inclusion 22 | Irregular | 250 × 115 | AOA | No | No | Olivine | Pyroxene | Absent |
| CAI 23 | Rectangular | 180 × 100 | Melilite-rich | Yes | Yes | Melilite | Spinel | Abundant |
| Inclusion 24 | Rhombus | 235 × 200 | AOA | No | No | Olivine | Pyroxene | Absent |
| Inclusion 25 | Irregular | 300 × 170 | AOA | No | No | Olivine | Pyroxene | Absent |
| CAI 26 | Irregular | 325 × 170 | Relict CAI in AOA? | No | No | Olivine | Spinel, pyroxene | Rare |
| CAI 37 | Tubular | 100 × 45 | Hibonite | No | No | Hibonite | Unidentified (Fe, Mg, Si-rich phase) | Rare |
| CAI 74 | Irregular | 130 × 40 | Hibonite | No | No | Hibonite | Unidentified (Fe, Mg, Si-rich phase) | Rare |

refractory composition, enriched in Al and Ca (Figure 4). However, corundum, hibonite, grossite and krotite were not found. A few of these (#1, 20) (Figure 4) also have fayalitic accretionary rim surrounding them while others seem to be nestled in a fine-grained matrix. A few representative CAIs are described in greater detail in the following paragraphs.

CAI #1: Is a rectangular-shaped object of $\sim 175 \times 100 \mu\text{m}$ that is predominantly composed of melilite along with several anhedral spinel grains of 1–20 μm size primarily concentrated in the periphery. Only a few (~ 7) rounded perovskite grains of 1–4 μm are also present in the central/core regions. The CAI has a Wark-Lovering (WL) rim sequence of 10–15 μm with a mineral layer sequence starting from the inward of spinel, melilite, pyroxene (titanium, aluminum-rich to Al-rich diopside). A very fine-grained $\sim 10 \mu\text{m}$ accretionary rim is also present. Comparisons of WL-rims between different CAIs and with other groups are discussed separately in later sections. Diopside layer of the WL-rim palisading the margins is quite Ti-rich ($\text{TiO}_2 \sim 8.5 \text{ wt}\%$). Absence of

perovskite associated with the basal spinel layer of WL-rim is another notable feature.

CAI #18: Is a near circular object, $\sim 235 \times 195 \mu\text{m}$ in size. It is also composed of gehlenitic melilite in addition to a significant abundance of anhedral spinel in the periphery, with several perovskite grains scattered mostly in the melilite closer to the margin. The Wark-Lovering rim sequence covers the entire convoluted surface of the inclusion. The rim sequence from inside outwards is constituted by $\sim 2\text{--}5 \mu\text{m}$ thick melilite, followed by $\sim 2 \mu\text{m}$ Ti-, Ca-rich pyroxene that is surrounded by a $\sim 10\text{--}15 \mu\text{m}$ thick rim of magnesian diopside. A few schreibersite (Fe, Ni)₃P grains are present below the WL-rims alongside perovskite. At the base of this rim sequence lies a layer of spinel which projects a few finger-like intrusions in melilite and it is difficult to discern if they are part of the rim or not. Figure 4 shows the linear profile of elemental oxide compositions across two transects traversing the CAI and WL-rim. The composition of the inner region is quite homogeneous over a distance of ~ 200 microns and is shown by the flat profile of Al_2O_3 , CaO, SiO_2 and MgO

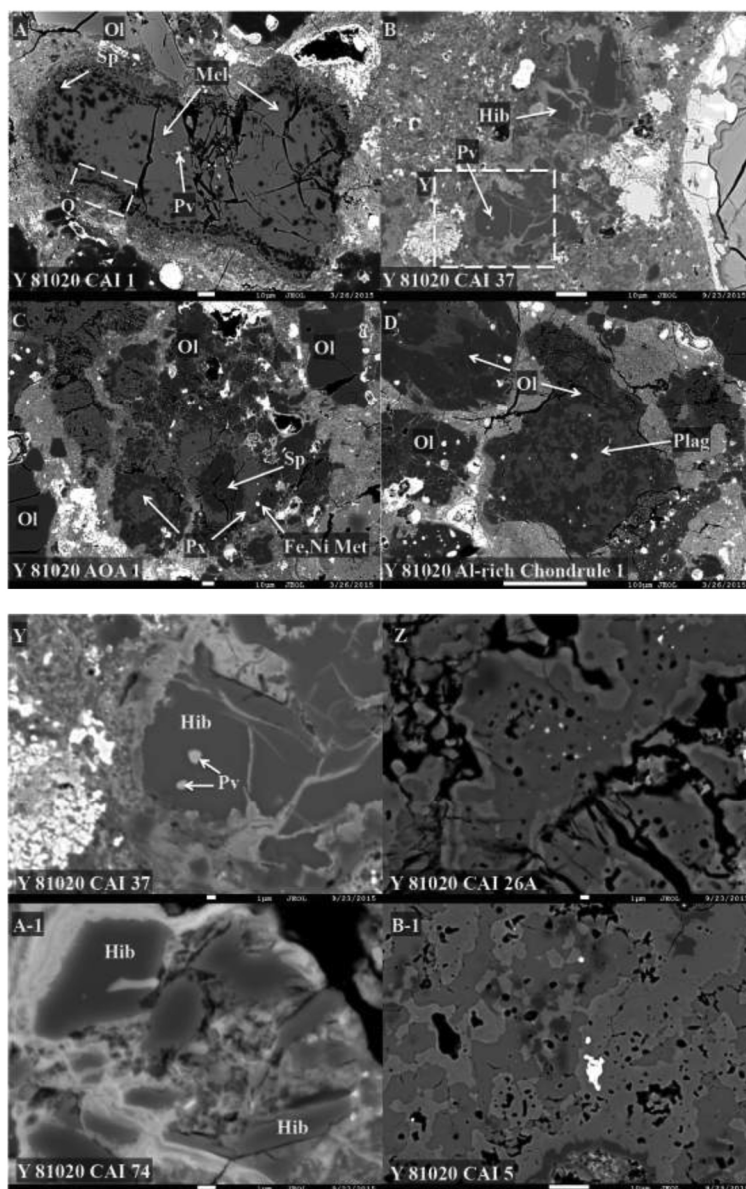


Figure 1. Back-scattered electron images of different types of objects in Y 81020 (CO3.05). Scale bars can be seen at the bottom of the image. Magnified images of the regions shown in dashed squares are shown separately (A) Melilite-rich kind of CAI with Wark-Lovering rim; (B) Hibonite inclusion; (C) Amoeboid olivine aggregate (AOA). Note the similarity (grey level) of olivine and spinel in the BSE image; (D) Al-rich chondrule. Y, Z, A-1, B-1, Magnified back scattered electron images of interior regions showing significant features of those object. Y, A-1, Rounded hibonite crystals from two different hibonite inclusions that have been altered at the periphery to Fe, Si, S, Zn rich unidentified phase. Z, Spinel–melilite–pyroxene inclusion. Note the dark coloured rounded spinel grain in the interior. Few small perovskite grains (bright coloured) are also seen. B-1, Spinel–anorthite–pyroxene inclusion. The dark coloured rounded grains in the interior are spinel. Few small perovskite grains (bright coloured) are also seen. Note the difference in size and shape of spinel grains in different types of CAIs.

(Figure 4 a). Figure 4 a also shows higher concentration of TiO_2 (5–8%) in the diopside layers and varying composition of different mineral phases in the WL-rim. The grey lines in Figure 2 show transects across this and other CAIs. Such a homogeneous composition in the inner region is indicated as #1 in Figure 2 and shown as transect 3 in Figure 4 b CMAS diagram plot at a single overlapping point. The data point being below the data points of other transects is not seen in Figure 4 b.

CAI #20: Is a $\sim 450 \times 245 \mu\text{m}$ large sea horse shaped refractory inclusion akin to CAI #18. The inclusion has fairly homogeneous composition unlike CAI #18. It has relatively less abundant, mostly anhedral spinel that are more evenly distributed within the inclusion. Perovskite grains are also fairly homogeneously distributed. The melilite is gehlenitic showing a clear trend of decreasing Al_2O_3 content from ~ 36 wt.% to 28 wt.% in the central region. There is corresponding increase in MgO content

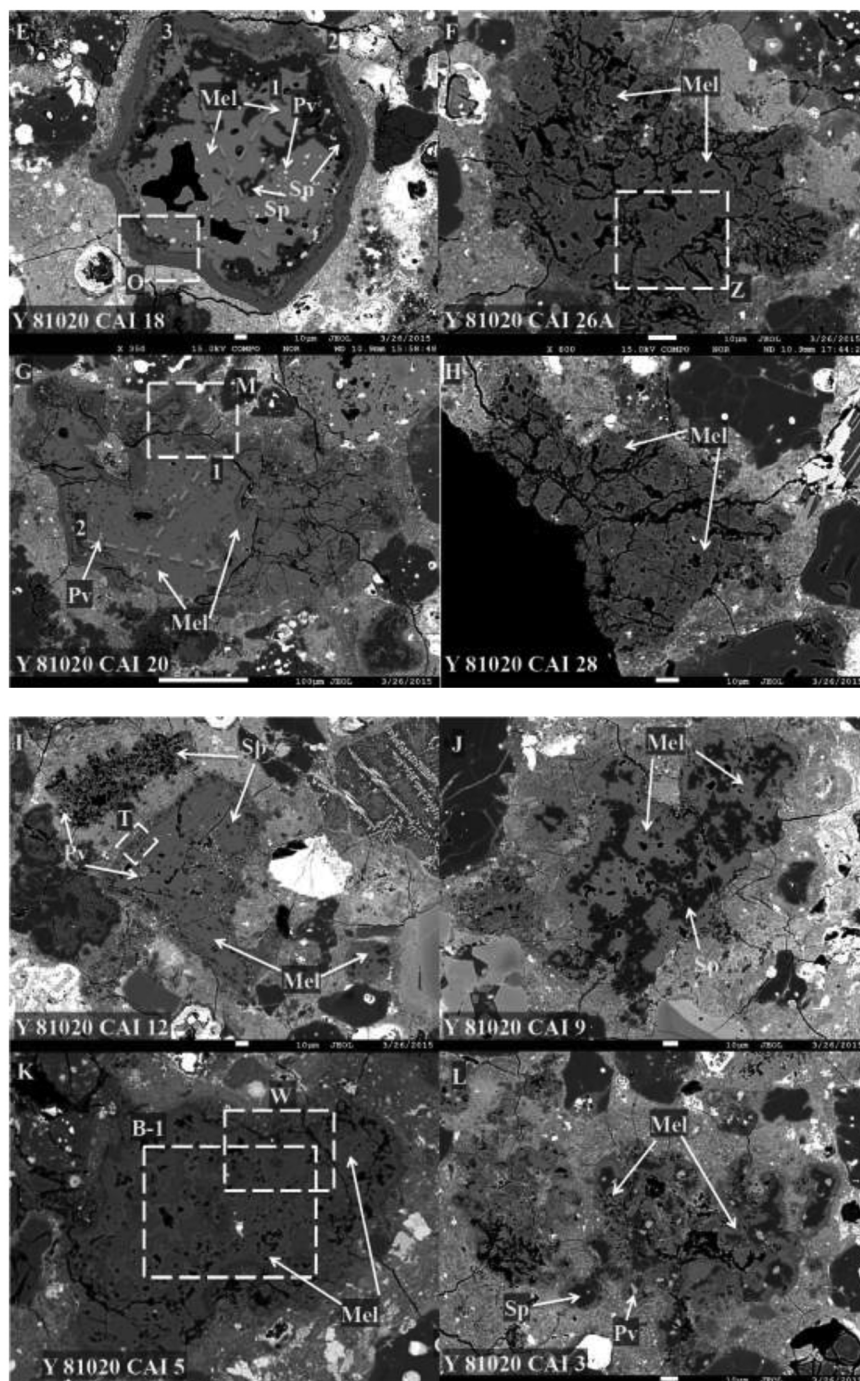


Figure 2. Back-scattered electron images of different types of CAIs in Y 81020 (CO3.05). Scale bars can be seen at the bottom of the image. Magnified images of the regions shown in dashed squares are shown separately. E, G, I show melilite-rich CAIs; F, H show spinel–melilite–pyroxene inclusions; K shows spinel–anorthite pyroxene inclusions; J, L show spinel–pyroxene inclusions.

from ~0.5 wt.% to ~3.5 wt.%. This can be interpreted in two ways: (1) crystallization from the periphery inward which would explain both the presence of spinel and more Al-rich phase in the outer regions. (2) Late stage evaporation of outer regions that evaporated most of the Mg, enriching Al and cooled rather quickly to explain the

texture of spinel. This was followed in a very short time by the formation of WL-rims. Both scenarios are equally plausible and can account for the mineralogical character and texture. Isotopic studies of Mg and Ca along with REE (rare earth elements) concentration profiles could possibly help discern between these two scenarios.

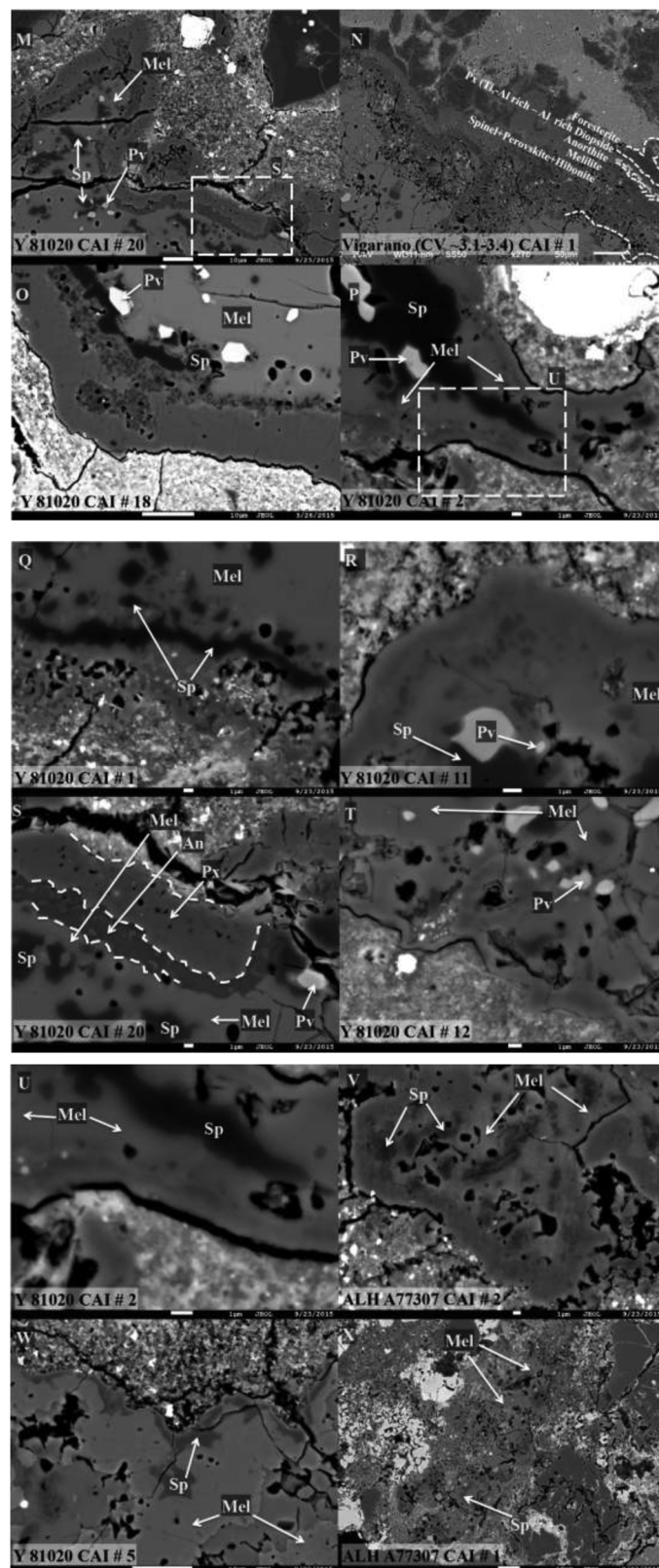


Figure 3. Back-scattered electron images of Wark-Lovering rims of CAIs in Y 81020 (CO3.05), Vigarano (CV~3.1–3.4), and ALH A77307 (CO3.03). Scale bars can be seen at the bottom of the image. Magnified images of the regions shown in dashed squares are shown separately in S and U. Magnified BSE images of selected regions of Wark-Lovering rims of CAIs in Y 81020 (CO3.05), and ALH A77307 (CO3.03) for melilite-rich kindered CAI are shown for lack of universality between two least altered meteorites of same type. Note the difference in scale bar between Y 81020 and Vigarano that shows the commonly observed, much thicker, more mono mineralic layers in Vigarano.

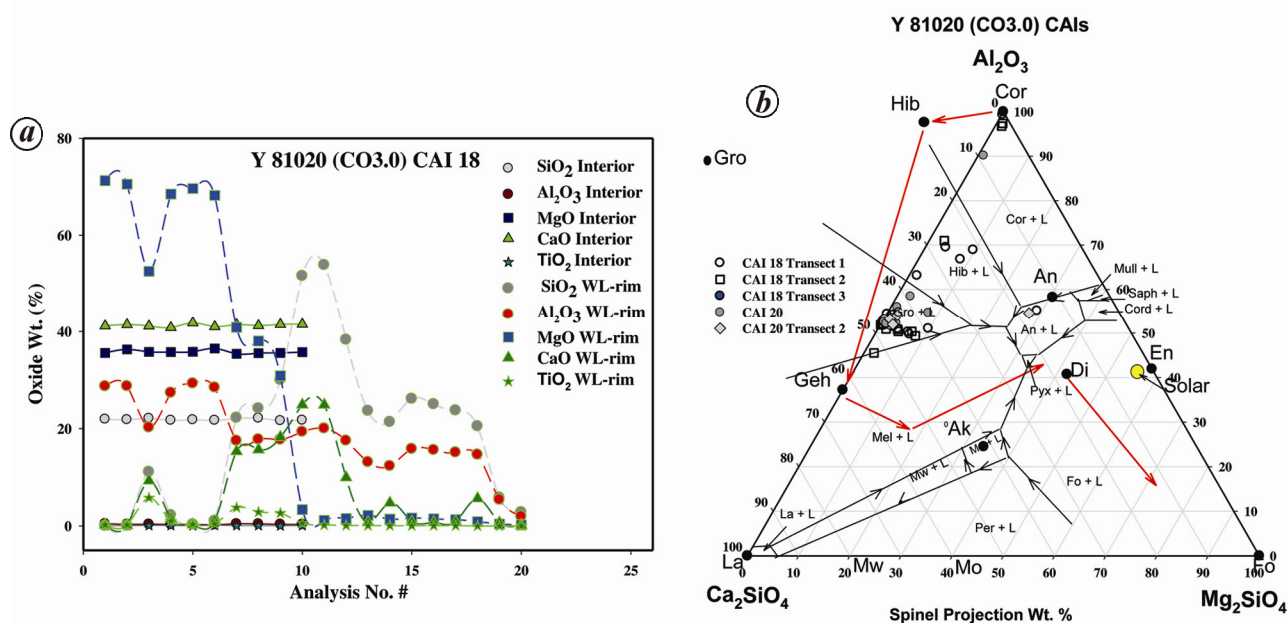


Figure 4. *a*, Variations in elemental (wt% oxide) compositions in the internal regions and across the WL-rim shown in Figure 2 of CAI #18. Note the uniformity in composition in the internal region over the distance of ~200 micron in melilite in CAI #18. This is in contrast to the significant gradient seen in Al₂O₃, MgO in other CAIs with the most significant gradient seen in one of the largest CAI #20. See text for details. *b*, Mineral composition of transects in CAIs (#20, 18) and some mineral phases (spinel, melilite, etc.) are shown in the spinel projected CMAS diagram. Two linear profiles of compositions, taken roughly perpendicular to each other across CAI #18, starting from below the WL-rim going from one end to the other end of the CAI. Line 1 in Figure 2 of CAI #18 is plotted as transect 3 in *b*. Transect 3 is the short linear profile made through the internal regions (~200 micron) shown in *a*. The uniform composition means all data points lie at a single place in the diagram and plot below the grey rhombus and not seen in the plot. Note for the other two perpendicular profiles, the variation between WL-rim, spinel plot along the expected regions.

However, these variations are in contrast to the homogeneous composition observed in CAI #18. This contrasting observation is however possible as different CAIs can experience different environments during their transport/residence in the solar nebula prior to incorporation in the parent body. The WL-rims are present along ~85% of the convoluted surface and the mono-mineralic layers are quite uniform in thickness around the inclusion. The inclusion is more fractured along one side and several physical cracks are present within the inclusions. The representative major mineralogy of the inclusion is given in Table 2 and transect profiles are plotted in Figure 4 *b*.

Spinel–melilite–pyroxene types

In the studied thin section these are typically smaller in size ~100 × 80 μm with each object consisting of several nodules which are sintered together to form respective objects. The nodules typically have perovskite in the core or at the edge of an anhedral spinel that is surrounded by melilite which in turn are mostly surrounded by a thin layer of pyroxene. These structures are quite similar to the previously described fine-grained spinel (pyroxene) rich CAIs in Efremovka and Vigarano except for the enrichment in Fe in some cases of Vigarano and Efremovka^{19,20}. Several spinel-rich inclusions in pristine CVs

have additional layers of melilite along with anorthite and pyroxene in these fine-grained CAIs¹⁹. The relative high abundance and compact texture of this type in Y 81020 is another differentiating factor compared to CV types in Efremovka and Vigarano. The relatively high abundance of spinel–pyroxene type in the studied section of Y 81020 may not be the general feature, as our comparative (unpublished) study of another pristine CO, ALH A77307 (3.03), does not show similar high abundance. This type shows further distinct feature of dichotomous abundance of perovskite. Half of spinel–pyroxene type inclusions have euhedral to anhedral perovskite grains in the core while the rest show the stark absence of them.

CAI #3: Is an irregular shaped, typical spinel–pyroxene type, ~100 × 70 μm in size. It has typical characteristics similar to several other (CAI #2, 4, 32C) shown in Figures 2–4. The size and abundance of perovskite grains vary quite significantly between these CAIs despite overall similar size of the inclusion. While CAI #2, 3, 32C have abundant perovskite grains, they are virtually absent in 9, 15, 17 exhibiting a clear trend of either their presence or their total absence. The sizes of spinel grains also show variability (less than a micron up to 10 microns) but they are mostly anhedral. While in CAI #3 spinel grains are less than 10 microns, these grains have sizes up to 15, 20 microns in CAI #2, 9 respectively. Compositionally

Table 2. Mineral compositions of the representative mineral phases in a few different kinds of objects

| Oxide wt% | CAI 1-1 Spinel | CAI 1 Melilite | CAI 1 Melilite | CAI 18 Spinel | CAI 18 Melilite | CAI 20 Spinel | CAI 20 Spinel | Al-rich Chond | Al-rich Chond | Refrac. Inclusion. #5 | Refrac. Inclusion. #5 | Refrac. Inclusion. #5 | Refrac. Inclusion. #5 |
|--------------------------------|----------------|--------------------|-----------------|---------------|-----------------|---------------|---------------|---------------------|----------------|-----------------------|-----------------------|-----------------------|-----------------------|
| Na ₂ O | BD | 0.02 | 0.02 | BD | BD | 0.04 | 0.01 | 0.07 | 0.05 | BD | BD | BD | BD |
| SiO ₂ | 1.15 | 25.53 | 22.95 | 0.35 | 21.1 | 11.71 | 0.16 | 42.49 | 47.1 | 36.99 | 46.57 | 25.35 | 8.69 |
| MgO | 28.43 | 11.58 | 1.2 | 28.55 | 1.98 | 19.47 | 28.75 | 0.43 | 49.64 | 48.26 | 15.86 | 18.15 | 24.48 |
| Al ₂ O ₃ | 67.8 | 35.12 | 33.76 | 71.38 | 36.09 | 52.09 | 70.86 | 36.68 | 0.34 | 0.64 | 8.99 | 36.64 | 58.13 |
| P ₂ O ₅ | 0.02 | 0.26 | 0.56 | BD | 0.6 | 0.15 | BD | 0.31 | BD | BD | 0.3 | 0.17 | 0.03 |
| K ₂ O | 0.01 | BD | 0.01 | 0.01 | BD | BD | BD | 0.01 | BD | 0.09 | BD | 0.02 | BD |
| CaO | 3.08 | 20.05 | 41.07 | 0.47 | 39.33 | 11.13 | 0.26 | 20.22 | 0.68 | 0.23 | 24.05 | 14.47 | 6.57 |
| TiO ₂ | 0.23 | 6.59 | 0.04 | 0.18 | 0.67 | 5.28 | 0.37 | 0.05 | 0.49 | 0.05 | 3.08 | 2.72 | 2.1 |
| Cr ₂ O ₃ | 0.38 | 0.18 | 0.06 | 0.12 | BD | 0.12 | 0.12 | 0.07 | 0.35 | 0.24 | 0.15 | 0.35 | 0.52 |
| MnO | 0.05 | BD | 0.08 | BD | 0.08 | BD | BD | 0.01 | 0.25 | 0.31 | BD | 0.1 | 0.03 |
| FeO | 0.23 | 1.33 | 0.21 | 0.2 | 0.12 | 0.4 | 0.21 | 0.16 | 1.44 | 13.15 | 0.62 | 0.66 | 0.51 |
| NiO | 0.03 | 0.31 | 0.07 | BD | BD | 0.08 | BD | 0.14 | BD | 1.05 | 0.09 | BD | BD |
| Total Phase | 101.43 Spinel | 100.98 Ca-pyroxene | 100.03 Melilite | 101.26 Spinel | 99.97 Melilite | 100.47 Spinel | 100.76 Spinel | 100.64 Plagio-clase | 100.33 Olivine | 101.01 Olivine | 99.72 Ca-pyroxene | 98.64 Ca-pyroxene | 101.05 Spinel |

Ca-Al-rich inclusions (CAIs) #1, 18, 20 are melilite-rich; Refractory inclusion (Refrac. Inclusion.) #5 is spinel–pyroxene type; Al-rich chondrule (Chond) #1.

most spinel grains were found to be closer to the MgAl₂O₄ end member. Bulk composition of this type lies in the same region as that of fine-grained spinel-rich CAIs in the CMAS diagram.

CAI #9: Is the other type of spinel–pyroxene inclusion showing distinct lack of perovskite grains. Others with similar texture and mineral characteristics include CAI #4, 15, 17, 21, etc. The spinel composition of this inclusion is similar to CAI #3 and near to MgAl₂O₄ end member. It is worthy to mention that all the types of CAIs are found in close vicinity of each other and with very little physical separation between them in the thin section.

Discussion

Comparison with refractory inclusions in other chondritic groups

Characterization and comparison of refractory inclusions and salient features of each of the different groups of meteorites particularly in CVs have been done earlier^{5,7,11–13,19}. Succinctly, in general, large (up to a few cm in size) CAIs with abundant mineral phases of melilite, spinel, anorthite and pyroxene have been found in CV types that have been altered to different degrees depending on the individual meteorite. On the other hand, more refractory minerals such as corundum, hibonite, spinel, perovskite and pyroxene are more dominant in CM types but have smaller sizes <400 μm. Other refractory minerals like grossite in CH/CB types, calcium aluminate in NWA 1934 (CV3) have been found restrictively in these meteorites. CR CAIs saliently show a higher degree of alteration despite very low limited aqueous alterations, in

general of matrices, chondrules, and other components of the meteorite. Typically CAIs are small in size and have lower abundance in CO types including Y 81020 compared to CVs.

Comparative analysis with other carbonaceous ornans type chondrites: general agreement in abundance and pristine character

Recent studies have classified ALH A77307 as another highly pristine meteorite. It is classified as CO3.03 compared to Y 81020 which has a petrographic type CO3.05. Previous studies and unpublished work on two sections of ALH A77307 note that Y 81020 has slightly higher abundance of CAIs. On the other hand, the largest size CAIs found in ALH A77307 are larger (~900 μm diameter) than the ones (<500 μm diameter) found in Y 81020. The CAIs in ALH A77307 in general have much thicker accretionary rims (~10–30 microns) with several CAIs having accretionary rims of ~50 μm compared to thin, incomplete rims in relatively fewer objects in the studied thin section of Y 81020. On the contrary, WL-rims were less abundant in ALH A77307 CAIs. There are fewer melilite rich CAIs in ALH A77307 which has more abundant fine-grained and melilite–spinel types. The outer margins of CAIs are surrounded with Fe-rich sulphides consistent with greater fluid mobilization in ALH A77307. This could be the rationale for greater abundance of fluids on the parent body of ALH A77307 when compared to the parent body of Y 81020. Kojima *et al.*¹³ compared the petrographic, mineralogical features of CAIs and refractory inclusions in three Antarctic meteorites (Y 81020, Y 82050, Y 790992) from CO3 and suggested increasing levels of alteration from Y 81020 < Y

82050 < Y 790992. Our observations are in agreement with previous studies suggesting pristine/unaltered characteristics of most of the inclusions in Y 81020.

Comparison of Wark-Lovering rims in different type of chondrites: a continuum (?) indicative of individual objects' recourse through nebula

Wark-Lovering rim sequence is $\leq 10\text{--}50\ \mu\text{m}$ (in total width) thick, distinct, concentric, mono/bi-mineralic sequence of mineral phases that are present in the outer margins, rather ubiquitously, of several CAIs in all types of chondrites. Typically, the inner most layer is spinel \pm hibonite \pm perovskite. This is followed outward by melilite and anorthite replacing melilite and pyroxene (grading from titanium, aluminium rich to aluminium diopside) and often surrounded by olivine layer^{21,22}. One or more of these layers may be absent in some CAIs but the WL-rim sequence faithfully follows the convoluted surface of CAIs in all types of chondrites. These mineral sequences are differentially altered due to local thermal, aqueous conditions in the nebular/parent bodies and hence show distinct characteristics typical in a meteorite. For example, the CV CAIs in Allende have suffered substantial aqueous alteration. Typically the melilite layer is replaced with a combination of nepheline–melilite and the outermost olivine/forsterite layer has been altered to hedenbergite, andradite with olivine and diopside. Figure 3 shows a typical WL-rim from Vigarano alongside Y 81020 and ALH A77307. In Y 81020 several small CAIs have WL-rims. The WL-rim composition is similar to the unaltered types found in Efremovka and Vigarano but with a few differences: (1) The outermost forsterite layer and melilite layer of WL-rim is missing in most of the CAIs (Figure 3 N, S); (2) The inner most layer has preponderance of spinel with limited distribution of perovskite along with paucity of hibonite; (3) The distinct WL-rims are typically present around melilite rich CAIs and are nearly absent in spinel pyroxene type. Figure 3 shows typical WL-rims around CAIs in Y 81020, Efremovka (CV), ALH A77307 and enlarged images of insets are shown in Figure 3 Q, S, U. In Y 81020, typical rim sequence is made up of relatively thick inner most layer of spinel with perovskite followed outwards by melilite, and pyroxene layer that show large variation from Ti–Al rich to Al rich diopside. This is wrapped by olivine layer. Subtle differences exist between rims around CAIs, mainly in the thickness, but there is notable near absence of WL-rim around spinel–melilite–pyroxene type. There is as yet incomplete understanding about WL-rims. Hence it is not clear whether the thin zonation seen around spinel–pyroxene type in Y 81020 and also in ALH A77307 represent the initiation or remnant of WL-rim. Figure 3 depicts these subtle variations and may be a continuum in the formation of WL-rims that each

individual CAI records during their residence in the Solar nebula.

Conclusions

Petrographic and quantitative studies of refractory inclusions in a representative thin section of Y 81020 showed different kinds of refractory inclusions. Based on their mineralogy and textural characteristics they have been classified into five different types and in general represent a wide gamut of mineral phases and textures each with their unique characteristics. There are several similarities and distinct features in Y 81020 compared to other chondrites. Most refractory inclusions show lack of evidence of alteration in concurrence with the previous suggestion of their pristine character.

1. Amelin, Y., Krot, A. N., Hutcheon, I. D. and Ulyanov, A. A., Lead isotopic ages of chondrules and calcium-aluminum-rich inclusions. *Science*, 2002, **297**, 1678–1683.
2. Bouvier, A. and Wadhwa, M., The age of the solar system redefined by the oldest Pb–Pb age of a meteoritic inclusion. *Nat. Geosci.*, 2010, **3**, 637–641.
3. Christophe Michel-Levy, M., Un chondre exceptionnel dans la meteorite de vigarano. *Bull. Soc. France Mineral. Crystallog.*, 1968, **91**, 212–214.
4. Grossman, L., Refractory inclusions in the Allende meteorite. *Annu. Rev. Earth Planet. Sci.*, 1980, **8**, 559–608.
5. MacPherson, G. J., Calcium–aluminum-rich inclusions in chondritic meteorites, In *Meteorites, Comets, and Planets, Treatise on Geochemistry* (ed. Davis, A. M.), Elsevier, 2007, vol. 1, pp. 201–246.
6. MacPherson, G. J., Simon, S. B., Davis, A. M., Grossman, L. and Krot, A. N., Calcium-aluminum-rich inclusions: Major unanswered questions. In *Chondrites and ProtoPlanetary Disk* (eds Krot, A. N., Scott, E. R. D. and Reipurth, B.), San Francisco, 2005, pp. 225–250.
7. Krot, A. N., Keil, K., Scott, E. R. D., Goodrich, C. A., Weisberg, M. K. and MacPherson, G. J., Classification of meteorites and their genetic relationships. In *Meteorites, Comets, and Planets, Treatise on Geochemistry* (ed. Davis, A. M.), Holland, H. D. and Turekian, K. K. (Executive editors), Elsevier, 2007, vol. 1, pp. 1–64.
8. Connolly, H. C. and Burnett, D. S., A study of the minor element concentrations of spinels from two type B calcium-aluminum-rich inclusions: An investigations into potential formation conditions of calcium-aluminum rich inclusions. *Meteorit. Planet. Sci.*, 1999, **34**, 829–848.
9. Connolly, H. C., Burnett, D. S. and McKeegan, K. D., The petrogenesis of type B1 Ca–Al-rich inclusions: The spinel perspective. *Meteorit. Planet. Sci.*, 2003, **38**, 197–224.
10. Simon, S. B., Davis, A. M., Grossman, L. and Zinner, E. K., Origin of hibonite-pyroxene spherules found in carbonaceous chondrites. *Meteorit. Planet. Sci.*, 1998, **33**, 411–424.
11. Russell, S. S., Huss, G. R., Fahey, A. J., Greenwood, R. C., Hutchison, R. and Wasserburg, G. J., An isotopic and petrologic study of calcium-aluminum-rich inclusions from CO3 meteorites. *Geochim. Cosmochim. Acta*, 1998, **62**, 689–714.
12. Russell, S. S., Davis, A. M., MacPherson, G. J., Guan, Y. and Huss G. R., Refractory inclusions from the ungrouped carbonaceous chondrites MAC 87300 and MAC 88107. *Meteorit. Planet. Sci.*, 2000, **35**, 1051–1066.

13. Kojima, T., Yada, S. and Tomeoka, K., Ca-Al-rich inclusions in three antarctic CO3 chondrites, Yamato-81020, Yamato-82050 and Yamato-790992: Record of low-temperature alteration. *Proc. NIPR Symp. Antarct. Meteorites*, 1995, **8**, 79–96.
14. Kimura, M., Grossman, J. N. and Weisberg, M. K., Fe-Ni metal in primitive chondrites: Indicators of classification and metamorphic conditions for ordinary and CO chondrites. *Meteorit. Planet. Sci.*, 2008, **43**, 1161–1177.
15. Grossman, J. N. and Brearley, A. J., The onset of metamorphism in ordinary and carbonaceous chondrites. *Meteorit. Planet. Sci.*, 2005, **40**, 87–122.
16. Bonal, L., Quirico, E., Bourot-Denise, M. and Montagnac, G., Determination of the petrologic type of CV3 chondrites by Raman spectroscopy of included organic matter. *Geochim. Cosmochim. Acta*, 2006, **70**, 1849–1863.
17. Bonal, L., Bourot-Denise, M., Quirico, E., Montagnac, G. and Lewin, E., Organic matter and metamorphic history of CO chondrites. *Geochim. Cosmochim. Acta*, 2007, **71**, 1605–1623.
18. Itoh, S., Kojima, H. and Yurimoto, H., Petrography and oxygen chemistry of Ca-, Al-rich inclusions in CO chondrites. LPSC 31, 2000, A#1323.
19. Mishra, R. K. and Chaussidon, M., Timing and extent of Mg and Al isotopic homogenization in the early inner Solar System. *Earth Planet. Sci. Lett.*, 2014, **390**, 318–326.
20. Krot, A. N., MacPherson, G. J., Ulyanov, A. A. and Pataev, M. I., Fine grained, spinel-rich inclusions from reduced CV chondrites Efremovka and Leoville: I. Mineralogy, petrology, and bulk chemistry. *Meteorit. Planet. Sci.*, 2004, **39**, 1517–1553.
21. Wark, D. A. and Lovering, J. F., Marker events in the early solar system: evidence from rims on Ca-Al-rich inclusions in the carbonaceous chondrites. Proc. 8th Lunar Sci. Conf., 1977, pp. 95–112.
22. Wark, D. A. and Boynton, W. V., The formation of rims on calcium aluminum-rich inclusions: Step I. Flash heating. *Meteorit. Planet. Sci.*, 2001, **36**, 1135–1166.

ACKNOWLEDGEMENTS. I thank D. K. Ross (JSC) for his assistance in carrying out electron probe work. I have benefitted from several scientific discussions with Justin I. Simon, K. K. Marhas, Marc Chaussidon and Jangmi Han. The work is supported by NASA Post-Doctoral Program (NPP) fellowship administered by Oak Ridge National Laboratory associated universities (ORAU), Tennessee, Kentucky.

Received 17 October 2015; revised accepted 22 November 2017

doi: 10.18520/cs/v114/i07/1510-1519